Acta Biomaterialia xxx (xxxx) xxx

Contents lists available at ScienceDirect

Acta Biomaterialia

journal homepage: www.elsevier.com/locate/actbio

Involvement of prenucleation clusters in calcium phosphate mineralization of collagen☆

Yu-xuan Ma[a,1], Samuel Edmund Hoff[b,1], Xue-qing Huang[c,1], Juan Liu[b], Qian-qian Wan[a], Qun Song[a], Jun-ting Gu[a], Hendrik Heinz[b,*], Franklin R. Tay[d,*], Li-na Niu[a,e,*]

[a] State Key Laboratory of Military Stomatology & National Clinical Research Center for Oral Diseases & Shaanxi Key Laboratory of Stomatology, Department of Prosthodontics, School of Stomatology, The Fourth Military Medical University, Xi'an, Shaanxi, China
[b] Department of Chemical and Biological Engineering, University of Colorado Boulder, Boulder, CO, USA
[c] Department of Prosthodontics, Guanghua School and Hospital of Stomatology, Guangdong Provincial Key Laboratory of Stomatology, Institute of Stomatological Research, Sun Yat-sen University, Guangzhou, Guangdong, PR China
[d] The Dental College of Georgia, Augusta University, Augusta, GA, USA
[e] The Third Affiliated Hospital of Xinxiang Medical University, Xinxiang, Hena, China

ARTICLE INFO

Article history:
Received 20 March 2020
Revised 15 July 2020
Accepted 17 July 2020
Available online xxx

Keywords:
Biomineralization
Donnan equilibrium
Interface force field
Intrafibrillar mineralization
Polymer-induced liquid precursors
Prenucleation clusters

ABSTRACT

Involvement of thermodynamically-stable prenucleation clusters (PNCs) in the biomineralization of collagen has been speculated since their existence was reported in mineralization systems. It has been hypothesized that intrafibrillar mineralization proceeds via nucleation of inhibitor-stabilized intermediates produced by liquid-liquid separation (*aka.* polymer-induced liquid precursors; PILPs). Here, the contribution of PNCs and PILPs to calcium phosphate intrafibrillar mineralization of collagen was examined in a model with a semipermeable membrane that excludes nucleation inhibitor-stabilized PILPs from reaching the collagen fibrils, using cryogenic electron microscopy of reconstituted fibrils and conventional transmission electron microscopy of collagen sponges. Molecular dynamics simulation with the Interface force field (IFF) was used to confirm the existence of PILPs with amorphous calcium phosphate and elucidate details of the dynamics. Furthermore, intrafibrillar mineralization of single collagen fibrils was experimentally observed with unstabilized PNCs when anionic/cationic polyelectrolytes were used to establish Donnan equilibrium across the semipermeable membrane. Molecular dynamics simulation verified PNC formation within the collagen intrafibrillar gap zones at the atomic scale and explained the role of external PILPs. The PILPs decrease the interfibrillar water content and increase the interfibrillar ionic concentration. Nevertheless, intrafibrillar mineralization of collagen sponges with PNCs alone was inefficacious, being constrained by competition from extrafibrillar mineral precipitation.

Statement of significance

Compared with conventional PILP-based intrafibrillar mineralization, mineralization of collagen fibrils using unstabilized PNCs is constrained by competition from extrafibrillar mineral deposition. The narrow window of opportunity for PNCs to produce intrafibrillar mineralization provides a plausible explanation for the feasibility of nucleation inhibitor-free intrafibrillar apatite assembly during reconstitution of type I collagen.

1. Introduction

Different *in vitro* models have been developed for rationalizing the mechanisms of intrafibrillar mineralization of calcium phosphate (CaP) in collagen [1–6], based on differential interpretations of the classical and nonclassical nucleation theories [7–9]. According to the classical nucleation theory, crystallization is predicated upon the stochastic association of ion clusters which are unstable with respect to dissolution. These precursors grow spontaneously by ion attachment and unit cell replication into crystals

☆ Part of the Special Issue on Biomineralization: From Cells to Biomaterials, associated with the BIOMIN XV: 15th International Symposium on Biomineralization, held at the Ludwig Maximilian University, Sept 9-13, 2019, organized by Wolfgang Schmahl and Erika Griesshaber.

* Corresponding authors.
E-mail addresses: Hendrik.Heinz@colorado.edu (H. Heinz), ftay@augusta.edu (F.R. Tay), niulina831013@126.com (L.-n. Niu).

[1] These authors contributed equally to this work.

https://doi.org/10.1016/j.actbio.2020.07.038
1742-7061/

with definitive lattice structures upon overcoming the interfacial free energy barrier between the supersaturated solution and the aggregate [10]. However, phenomena such as involvement of disordered CaP phases in biogenic mineralization, presence of stable (metastable) prenucleation clusters (PNCs) in inorganic mineral salt solutions, and ordered aggregation of mesocrystals in crystal growth are not readily accountable by the classical nucleation theory [11–13].

Two-step and multi-step nucleation models based on the non-classical crystallization pathway have been introduced to account for these phenomena [14,15]. According to these models, minerals do not crystallize directly into the most thermodynamically-stable phase. Instead, intermediate phases are formed in ionic species-crowded solutions, generating PNCs and subsequently, increasingly-densified hydrated intermediates, for participation in the crystallization chain of events [16]. This chain of events has also been identified in crystallization of CaP. Using cryogenic-electron microscopy (cryo-EM), Dey et al. [17] reported that surface-induced apatite precipitation from simulated body fluid was initiated by speciation beyond ion pairs, analogous to the "Posner's clusters" of highly-hydrated calcium phosphate in the classical crystallization pathway; the latter densified into metastable amorphous nanodroplets via liquid-liquid demixing and subsequently nucleate and grow into crystalline phases. Other forms of CaP prenucleation species have been reported in the literature [18–22]. These PNCs may represent different stages of speciation development during densification into hydrated amorphous calcium phosphate (ACP). The philosophical discovery of PNC and its role in biomineralization appear to have bridged the gap between classical and non-classical nucleation theories [9,23].

Liquid-liquid separation of densified, hydrated PNCs by spinodal decomposition represents an alternative route of mineralization [24–26]. Such a process is notably identified in calcium carbonate mineralization systems. Phase separation occurs spontaneously via diffusion, in the absence of a thermodynamic barrier, when the concentration of the increasingly densified PNCs crosses the unstable spinodal within the miscibility gap of an isobaric phase diagram (temperature vs composition) of a binary solvent-solute system [27]. In the absence of a stabilizing agent, this alternative mode of liquid densification readily coalesces into a hydrated liquid mineral intermediate that eventually solidifies upon the loss of hydration water. Introduction of a polyelectrolyte additive does not alter the liquid-liquid binodal limit of the solvent-solute system, but probably inhibits the sequestration of hydration water or stabilizes the nanodroplets colloidally against aggregation or dehydration [28]. Liquid-liquid phase separation intermediates that are stabilized by matrix proteins or their biomimetic nucleation-inhibiting analogs [29] have been coined polymer-induced liquid precursors (PILPs) [30]. The existence of PILPs has been challenged in a recent cryo-EM study [31], however, cryo-TEM is arguably a snapshot procedure that does not account for the dynamic nature of these intermediates. Unmistakably, PILP is revolutionary as a crystallization concept for calcium carbonate, CaP-based mineralization systems and other non-calcium based systems [32,33]. For CaP-based mineralization systems, polyelectrolyte stabilization of amorphous CaP mineralization precursors is important for intrafibrillar mineralization of collagen because the process does not occur in the absence of polymeric process-directing agents except under extreme hyperosmolarity [5,8].

Because PNCs are the smallest aggregates identified from CaP mineralization systems and are formed in solutions irrespective of the presence of nucleation inhibitors [3,17], one may envisage them, or their increasingly-densified hydrated intermediates, as the primary precursor species in the intrafibrillar mineralization process. This is logical from a bottom-up nano-engineering perspective because PNCs (~0.87 nm in diameter) [17] are smaller than the spacings between triple helical strands (~1.5 nm) within a collagen microfibril [34]. Individual entities can enter those spaces directly without relying on the larger shape-adaptable, polyelectrolyte-stabilized PILP particulates [35].

Despite the perceivably well-defined role of PNC as solute precursors in crystallization [36], the relative contribution of PNC in intrafibrillar mineralization of collagen fibrils by CaP systems is unknown. A major hurdle that undermines such investigations is the lack of an appropriate experimental model that distinguishes the thermodynamically-stable PNCs from nucleation inhibitor-stabilized PILPs produced via spinodal decomposition. This hurdle was resolved experimentally in the present study by using an *in vitro* model of a semipermeable membrane to establish Donnan equilibrium, and to restrict the passage of cationic or anionic polyelectrolyte nucleation inhibitors through the semipermeable membrane to produce stabilized PILPs during collagen biomineralization. The experimental results were validated using molecular dynamics simulation (MDS), which allow critical insights into PNC speciation and growth [28,37–40]. Specifically, we utilized the Interface Force Field (IFF) along with CHARMM36 that contains calcium phosphate models with quantitative validation of aqueous interfacial properties across a range of pH values [41–43]. The hypothesis tested was that collagen intrafibrillar mineralization may be achieved using hydrated PNCs within normal physiological range, under the condition that inhibitors establish electrical neutrality and osmotic equilibrium across a semipermeable membrane.

2. Material and methods

2.1. Materials

Poly(allylamine) hydrochloride (PAH, Mw 17.5 kDa), calcium chloride dihydrate ($CaCl_2$•$2H_2O$), sodium phosphate dibasic (Na_2HPO_4) and fluorescamine were purchased from MilliporeSigma (St. Louis, MO, USA). Poly-L-aspartic acid sodium salt (PAsp, Mw 27 kDa) was purchased from Alamanda Polymers (Huntsville, Alabama, USA). All chemicals were used as received. Dialysis tubing kit with molecular weight cut-off (MWCO) of 500 Da was purchased from Spectrum Laboratories, Inc. (Rancho Dominguez, CA, USA). Additional details of the materials employed, experimental, and computational procedures can be found in Supplementary Information SI-1.

2.2. Gel permeation chromatography (GPC)

For selection of semipermeable membranes with an appropriate molecular weight cut-off (MWCO), molecular weight distributions of the commercially-acquired PAsp and PAH were first determined using GPC. Molecular weight distributions of the PAH and PAsp were examined using GPC as described in SI-1.

2.3. Fluorescamine assay

Because of the higher polydispersity index of PAH compared with PAsp, fluorescamine assay was used to confirm the absence of the polycationic electrolyte from the interior of the semipermeable membrane tubing as described in SI-1.

2.4. Experimental setup

For the experimental groups, PAsp and PAH were used respectively as the polyanionic [44] or polycationic [6] nucleation inhibitor for the CaP mineralization system. Each nucleation inhibitor was mixed with a calcium source (9 mM $CaCl_2$•$2H_2O$) that was separated from the phosphate source (4.2 mM Na_2HPO_4) by a

semipermeable membrane. The latter enabled free diffusion of water molecules, calcium and phosphate ionic species but prevented migration of the PAsp or PAH from the calcium side of the membrane to the phosphate side. The volume of solution inside and outside the dialysis bag was 15 mL, respectively.

For the negative control group, a calcium source (9 mM $CaCl_2$•$2H_2O$) was separated from the phosphate source (4.2 mM Na_2HPO_4) by a semipermeable membrane to generate supersaturated CaP solution (4.5 mM $CaCl_2$ and 2.1 mM Na_2HPO_4 in HEPES buffer) without incorporating a nucleation inhibitor outside the dialysis tubing to establish Donnan equilibrium [6].

For the positive control group, polyelectrolyte-stabilized CaP amorphous intermediates were prepared by rapid mixing of equal volumes of 9 mM $CaCl_2$ and 4.2 mM Na_2HPO_4 in HEPES buffer at room temperature and adding PAH or PAsp to achieve a final PAH concentration of 500 μg/mL or PAsp concentration of 75 μg/mL. No dialysis tubing was used in the positive controls.

2.5. Cryogenic-electron microscopy (cryo-EM) and transmission electronic microscopy (TEM)

Mineralization of the collagen grids and sponges (size: 5 mm × 5 mm × 2 mm; Ace Surgical Supply, Brockton, MA, USA) was examined by cryo-EM and TEM, respectively. Briefly, gold grids with holey-carbon supporting films were used for surface-deposition of reconstituted rat-tail type I collagen fibrils. For the experimental and the negative control groups, mineralization was performed by placing the grids/sponges ($N = 3$) inside a sealed dialysis tubing containing the phosphate solution. The assembly was immersed in an equal volume of calcium solution with/without inhibitors, with constant slow stirring at 37 °C for 7 days. For the positive groups, the grids/sponges ($N = 3$) were placed in the mixed solution previously described directly. The grids were retrieved after 1, 4 or 24 h and vitrified in liquid ethane for cryo-EM to observe the early stages of mineralization of single-layer collagen fibrils (SI-1). Mineralized collagen sponges retrieved from dialysis tubing were embedded in epoxy resin. Ninety nanometer-thick sections were prepared using an ultramicrotome and examined without staining, using a JEM-1230 transmission electron microscope (JEOL, Tokyo, Japan) at 110 kV.

2.6. Molecular dynamics simulations with the interface force field (CHARMM-IFF)

Molecular dynamics simulations (MDS) with CHARMM36-IFF were used to explain the mechanism of PNC formation from the molecular scale to the experimental scale [28,41,42]. To understand the tendency for PNC formation, the concentrations of water and ions inside and outside a collagen fibril were analyzed in the absence or presence of PAsp and PAH outside a semipermeable membrane. The local ionic concentrations are expected to correlate with the propensity of PNC formation. Hence, an overall concentration of 4.5 mM Ca^{2+} ions (2.1 mM HPO_4^{2-} ions), as well as a highly-supersaturated concentration (0.5 M Ca^{2+}, 0.23 M HPO_4^{2-} with a fixed Ca^{2+}:HPO_4^{2-} ratio of 4.5:2.1, same as experimental condition) were used in the MDS to distinguish trends in the formation of PNCs at a time scale of nanoseconds that is much shorter than typical experiments (SI-1). Additional detailed methods of the different molecular dynamics simulations can be found in the SI.

2.7. Statistical analysis

Data were presented as means ± standard deviations. For the fluorescamine assay, the concentrations of PAH outside the dialysis tubing before and after dialysis were analyzed using Student *t*-test, with statistical significance pre-set at $\alpha = 0.05$. All the experiments were performed in triplicate.

3. Results and discussion

The rationale of the present *in vitro* model was to use a semipermeable membrane to establish Donnan equilibrium, and to restrict the passage of cationic or anionic polyelectrolyte nucleation inhibitors through the membrane to produce stabilized PILPs during collagen biomineralization. To fulfill this experimental setup, GPC was used to select the membrane MWCO. Based on the GPC results (SI-2), dialysis tubing with 500 Da MWCO was used for subsequent experiments. Calcium ions (40.08 Da) and hydrogen phosphate ions (95.80 Da) are small enough to diffuse in and out of the dialysis tubing with 500 Da MWCO, whereas the bulkier nucleation inhibitor molecules are prevented from entering the tubing.

Because of the higher polydispersity index of PAH compared with PAsp, fluorescamine assay was used to rule out the possibility that the small molecules of the polymer may manage to pass through the dialysis tubing to generate PILP inside the tubing. Results of the assay indicated that PAH could be successfully blocked by the tubing (SI-3). Because size exclusion of polyelectrolytes from the interior of the tubing prevented PILPs from forming, collagen fibrils within the confines of the semipermeable membrane could only be mineralized by the thermodynamically-stable PNCs.

When PAsp was placed outside the semipermeable membrane, collagen fibrils on grids retrieved after 1 h were not yet mineralized (Fig. 1a). Random distribution of PNCs could be identified in the vitrified solution and around the unmineralized fibrils (Fig. 1b). The first sign of intrafibrillar mineralization was observed after 4 h (Fig. 1c). After 24 h, more intense intrafibrillar mineralization was evident in some fibrils, together with mineral precipitation around the fibrils (Fig. 1d). At high magnification, electron-dense intrafibrillar minerals could be seen in the partially-mineralized collagen fibrils (Fig. 1e). Extrafibrillar precipitations were observed around the more heavily-mineralized fibrils (Fig. 1f). These hydrated precipitations had not yet acquired the platelet/needle-shaped morphology of dehydrated extrafibrillar crystallites seen in conventional TEM (see below). Similar cryo-EM observations were identified when PAH was placed outside the dialysis tubing (not shown).

Mineralization of the single-layer collagen in the presence of PILPs (positive control), without the confines of a semipermeable membrane, was also examined with cryo-EM. Unlike the experimental medium in the semipermeable membrane system, there were no temporal changes in ionic concentration within this control mineralization medium. After 1 h of immersion, PNCs as well as larger PAsp-stabilized liquid-liquid phase-separated CaP precursors were randomly distributed among the unmineralized collagen fibrils (Fig. 1g). In specimens retrieved after 4 h of immersion, the intrafibrillar spaces within the collagen fibril were filled with amorphous minerals (Fig. 1h). Fully-mineralized collagen fibrils were identified in 24-hour specimens (Fig. 1i). Similar results were achieved using PAH as nucleation inhibitor (not shown).

Because the Ca^{2+} and HPO_4^{2-} ions were initially present on the opposite sides of the semipermeable membrane, one may envisage that there will be a temporal change in ionic concentrations in the solutions inside and outside the membrane (Fig. 2). Within the confines of the membrane where mineralization occurs, a gradual increase in the concentration of both ions occurred. Simulations also indicate outflux of some water from the dialysis tubing. However, experimental osmolality measurements have been difficult to measure in such a minute mineralization system. The process has some similarity to the use of PEG to concentrate proteins [45]. After the PNCs are formed, they densify and coalesce into nanodroplets when their ion activity product reaches a

Please cite this article as: Y.-x. Ma, S.E. Hoff and X.-q. Huang et al., Involvement of prenucleation clusters in calcium phosphate mineralization of collagen, Acta Biomaterialia, https://doi.org/10.1016/j.actbio.2020.07.038

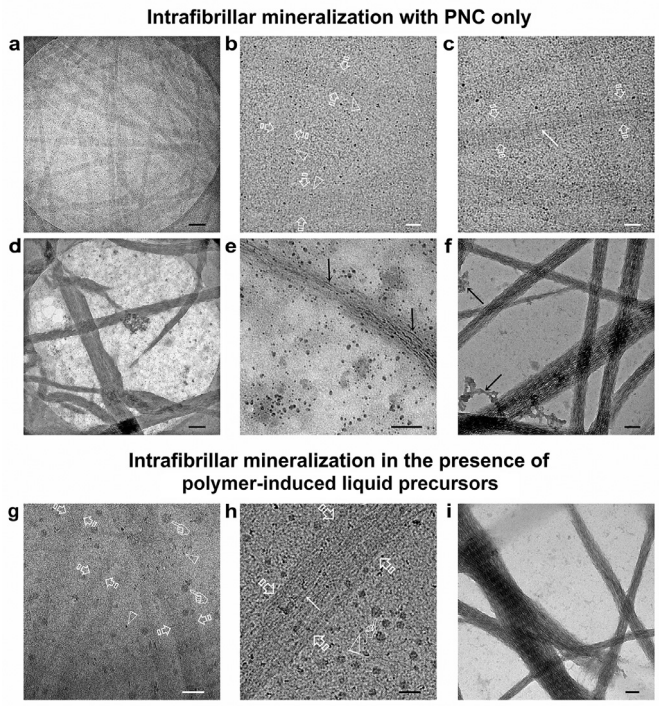

Fig. 1. Cryo-EM of intrafibrillar mineralization of single-layer collagen fibrils with **a-f**. PAsp placed outside the semipermeable membrane, and **g-i**. the use of PAsp as nucleation inhibitor for formation of CaP-PILPs in the absence of a semipermeable membrane (control). **a**. A grid that was retrieved from the dialysis tubing after 1 h (bar: 200 nm). Collagen mineralization was not apparent at this stage. **b**. High magnification of the 1-h specimen (bar: 50 nm) showing random distribution of PNC (open arrowheads) in solution and around the unmineralized fibrils (between open arrows). **c**. High magnification of a 4-h specimen (bar: 50 nm). Intrafibrillar spaces within the collagen fibril (between open arrows) were filled with amorphous material (arrow). **d**. A grid that was retrieved after 24 h (bar: 200 nm). Intrafibrillar mineralization was apparent in some fibrils and crystalline precipitation could be seen around the fibrils. **e**. High magnification of a partially-mineralized collagen fibril in the 24-h specimen (bar: 100 nm). Electron-dense intrafibrillar crystalline phase transformation occurred in some parts of the fibril (arrows). **f**. High magnification of fully-mineralized collagen fibrils in a 24-h specimen (bar: 100 nm) with extrafibrillar precipitations around the fibrils (pointers). **g**. High magnification of a 1-h specimen (bar: 50 nm) showing PNCs (open arrowheads) and larger PAsp-stabilized amorphous CaP intermediates (pointers). These intermediates, probably representing PILPs, were randomly distributed among unmineralized collagen fibrils (between open arrows). **h**. High magnification of a 4-h specimen (bar: 50 nm). Intrafibrillar spaces within the collagen fibril (between open arrows) were filled with amorphous minerals (arrow). Inset: selected area electron diffraction taken from open arrowed location of the collagen fibril reveals the amorphous nature of the infiltrated minerals. Pointer: PAsp-stabilized amorphous CaP intermediates (pointers); Open arrowheads: PNCs. **i**. High magnification of fully-mineralized collagen fibrils in a 24-h specimen (bar: 100 nm).

point where the liquid-liquid bimodal is crossed, initiating demixing. As the concentration of the HPO_4^{2-} ions continues to increase by diffusion within the membrane, the CaP mineralization medium within the membrane reaches a degree of supersaturation where the spinodal limit is exceeded, resulting in spontaneous liquid-liquid phase separation. Even if the degree of supersaturation cannot proceed to the spinodal point because of the consumption of Ca^{2+} and HPO_4^{2-} ions between the binodal (B) and spinodal (S) points, liquid-liquid phase separation intermediates, because of their liquid-like characteristics can pass through the pores of the membrane after dissociating themselves from the nucleation inhibitor along the membrane interface. While one cannot ignore the contribution of this alterative liquid mineral phase in intrafibrillar mineralization of the collagen fibrils, it is likely that these dense liquid CaP droplets rapidly crystallize and precipitate outside the fibrils, in the absence of nucleation inhibitor stabilization, before they can infiltrate the internal milieu of the collagen fibrils. Moreover, the intrafibrillar spaces are presumably occupied by PNCs and their increasingly-densified hydrated intermediates at this time.

The feasibility of intrafibrillar mineralization with PNCs was interrogated with further experiments, using 3-D collagen sponges prepared from reconstituted bovine type I collagen. Unlike a 2-D layer of widely separated collagen fibrils, these 3-D sponges require considerably more time to be mineralized (Fig. 3). Because the mineralized sponges required sectioning for viewing, thin sections of epoxy resin-embedded specimens that had been mineralized for 7 days using the same experimental set-up were prepared by ultramicrotomy and examined unstained using conventional TEM. High-resolution TEM images can be found in the supplementary information (SI-4). For the PAsp system, collagen sponges were typically partially-mineralized, in the form of nodules within the sectioned collagen leaflets, with large crystalline deposits along the leaflet surface (Fig. 3a, left). Within a nodule of mineralization (Fig. 3a, middle), mineralized fibrils with cross-banding patterns could be identified (Fig. 3a, right). Similar features were identified in the PAH system. Typically, collagen leaflets within the sponges were partially-mineralized in longitudinal sections, with large extrafibrillar crystalline deposits along the leaflet surface (Fig. 3b, left). Nodules of intrafibrillar mineralization could be identified in sections that were cut transversely (Fig. 3b, middle). Within the nodule, intrafibrillar minerals were orderly-aligned, producing cross-banding patterns along the fibril's longitudinal axis (Fig. 3b, right). Selected area electron diffraction of mineralized fibrils yielded ring-shaped diffraction patterns that were characteristic of hydroxyapatite.

For comparison with PILP-initiated intrafibrillar mineralization, controls were conducted by mineralizing collagen sponges with PAH-stabilized or PAsp-stabilized CaP mineralization precursors, in the absence of a semipermeable membrane. When PAsp was used directly as nucleation inhibitor to produce PILPs, heavily-mineralized collagen leaflets were seen by TEM after 7 days (Fig. 3c, left). At high magnification, intrafibrillar mineralization was apparent in longitudinally- sectioned (Fig. 3c, middle) and transversely-sectioned collagen fibrils (Fig. 3c, right). Similar results were achieved when PAH was used to stabilize PILPs in the absence of dialysis tubing (not shown).

Molecular dynamics simulations (MDS) with the CHARMM-IFF force field were employed to better understand the mechanism of PNC formation from the molecular scale to the experimental scale [28,41,42]. The local concentrations of water and ions inside and outside a collagen fibril were analyzed in the absence or presence of PAsp and PAH to interrogate possible correlations with the formation of PNCs (Fig. 4). The polymers were located outside a semipermeable membrane. The collagen model represents a fragment of a previously derived human collagen model [6] and was represented by 24 strand fragments of approximately 18 amino acid-length (SI-1). The amino acid composition of this section is considered representative although minor variations relative to other domains or alternative sequences are possible. An overall concentration of 4.5 mM Ca^{2+} ions (2.1 mM HPO_4^{2-} ions), as well as a highly-supersaturated concentration of 0.5 M Ca^{2+} (0.23 M HPO_4^{2-} ions) with a fixed Ca^{2+}:HPO_4^{2-} ratio of 4.5:2.1, similar to the experimental conditions, were used in the MDS to monitor trends in the formation of PNCs in collagen containing systems in all-atom resolution. With respect to limitation, the simulations are restricted to a local scale of ~20 nm that is much smaller than the experimental setup of millimeters. The atomistic models nevertheless provide a good approximation of the experimental conditions because (1) the concentrations of ions and polymers are the main drivers for the mineralization behavior and comparable between simulation and experiment, (2) the distance between the membrane/PILP and the collagen fragment of >10 nm

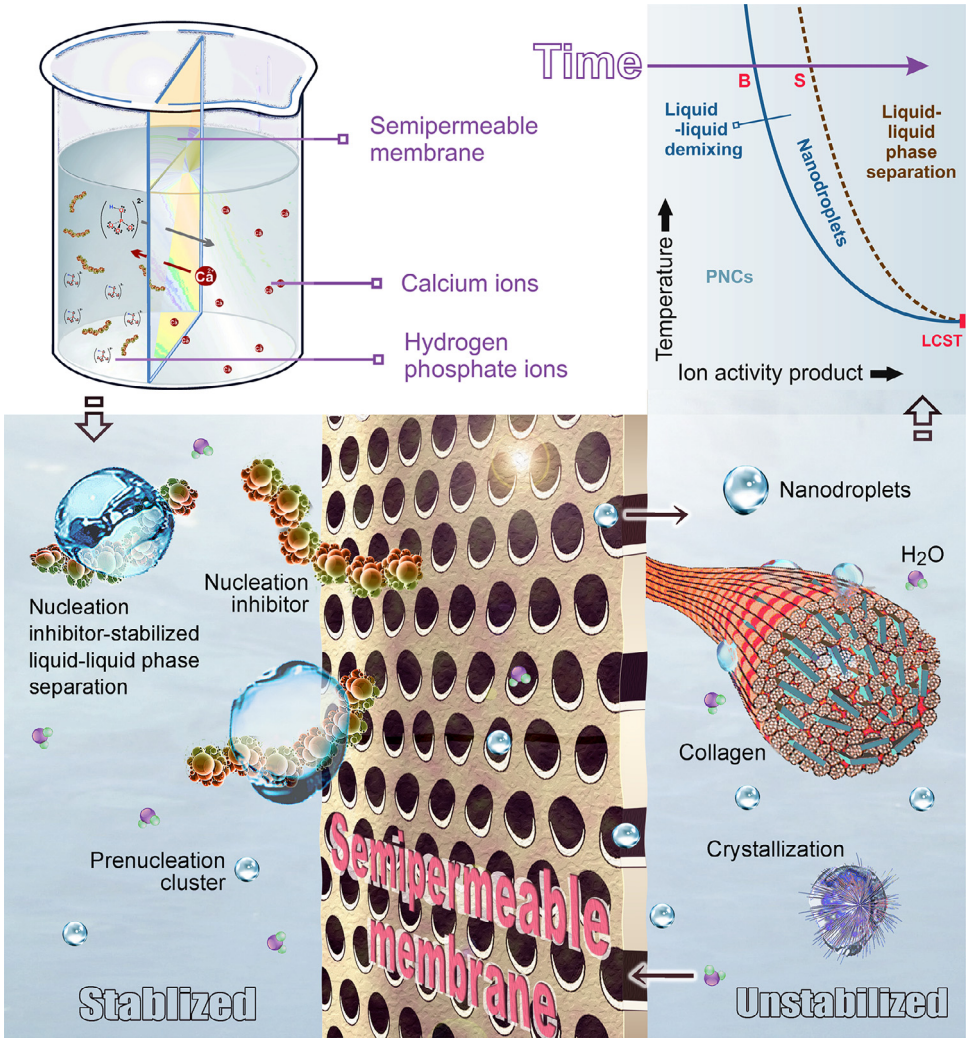

Fig. 2. Schematic depicting speciation of CaP amorphous intermediates outside and within the confines of a semipermeable membrane where collagen mineralization occurs. The top of the schematic (on the right side of the semipermeable membrane) is an arbitrary binary phase diagram, adapted from the speciation for aqueous calcium carbonate solution, which illustrates the changes in speciation with time within the semipermeable membrane. Abbreviations - B: liquid-liquid bimodal; S: spinodal; LCST: lower critical solution temperature.

in the simulation is greater than the range of intermolecular and electrostatic forces in solution (Fig. 4). Specifically, van-der-Waals interactions reach ~1.2 nm distance and electrostatic interactions up to ~3 nm in an overall electroneutral ionic solution in the absence of significant charge separation or externally applied electric fields [43]. Therefore, the model dimensions in MDS were sufficient to largely eliminate bias in the observed dynamics. The time scale of 100 ns in the simulations is also much shorter than in typical experiments. However, it is sufficient to monitor conformations and CaP prenucleation at high supersaturations at the nanometer length scale. Semi-quantitative correlations with experiments are therefore possible despite limitations in the accessible length and time scales in the simulations (see methods in SI-1)."

The Ca^{2+} and HPO_4^{2-} ions were uniformly distributed in the polymeric nucleation inhibitor-free solution (Fig. 4a). Introduction of PAH outside the semipermeable membrane increased the concentration of HPO_4^{2-} ions in the immediate vicinity to a higher level than in the free solution due to the positive charge (+20 e) (Fig. 4b and inset). Approximately 10 HPO_4^{2-} ions were attracted as nearest neighbors to PAH (within 3 Å), due to stronger binding of HPO_4^{2-} ions compared to Cl^- ions that originally compensated the positive charge. A smaller number of HPO_4^{2-} ions around PAH, compared to Ca^{2+} ions around PAsp (Fig. 4c and inset) is related to the larger size of the hydrogen phosphate anions. Introduction of PAsp outside the membrane increased the local concentration of Ca^{2+} ions due to the negative charge (−20 e) and stronger binding to Ca^{2+} ions than to Na^+ ions that originally compensate the charge of PAsp (Fig. 4c and inset). A total number of 14 Ca^{2+} ions and no other cations were directly bound to PAsp within 3 Å distance on time average (additional information in SI-5).

Changes in ionic distribution outside the semipermeable membrane influenced the space inside the membrane and the collagen intrafibrillar space. The presence of PAH and PAsp with the attached ionic shells outside the membrane reduced the water content in the intrafibrillar space and increased the concentration (number) of HPO_4^{2-} ions inside the collagen fibril (Fig. 4g). At lower concentration (4.5 mM Ca^{2+}, 2.1 mM HPO_4^{2-}), the decrease in intrafibrillar water content was approximately 4.5 ± 1% in the PAH-containing system and 10±2% in the PAsp-containing system, qualitatively in proportion to their capacity to scavenge divalent ions and their hydration shells from within the membrane. As a result, the concentration of ions in the intrafibrillar space increased (Fig. 4d–f), conducive to faster nucleation and formation of PNCs. In addition, the amount of HPO_4^{2-} ions in the intrafibrillar space also slightly increased in the presence of external PAsp and PAH, further accelerating PNC formation. The absolute number

Please cite this article as: Y.-x. Ma, S.E. Hoff and X.-q. Huang et al., Involvement of prenucleation clusters in calcium phosphate mineralization of collagen, Acta Biomaterialia, https://doi.org/10.1016/j.actbio.2020.07.038

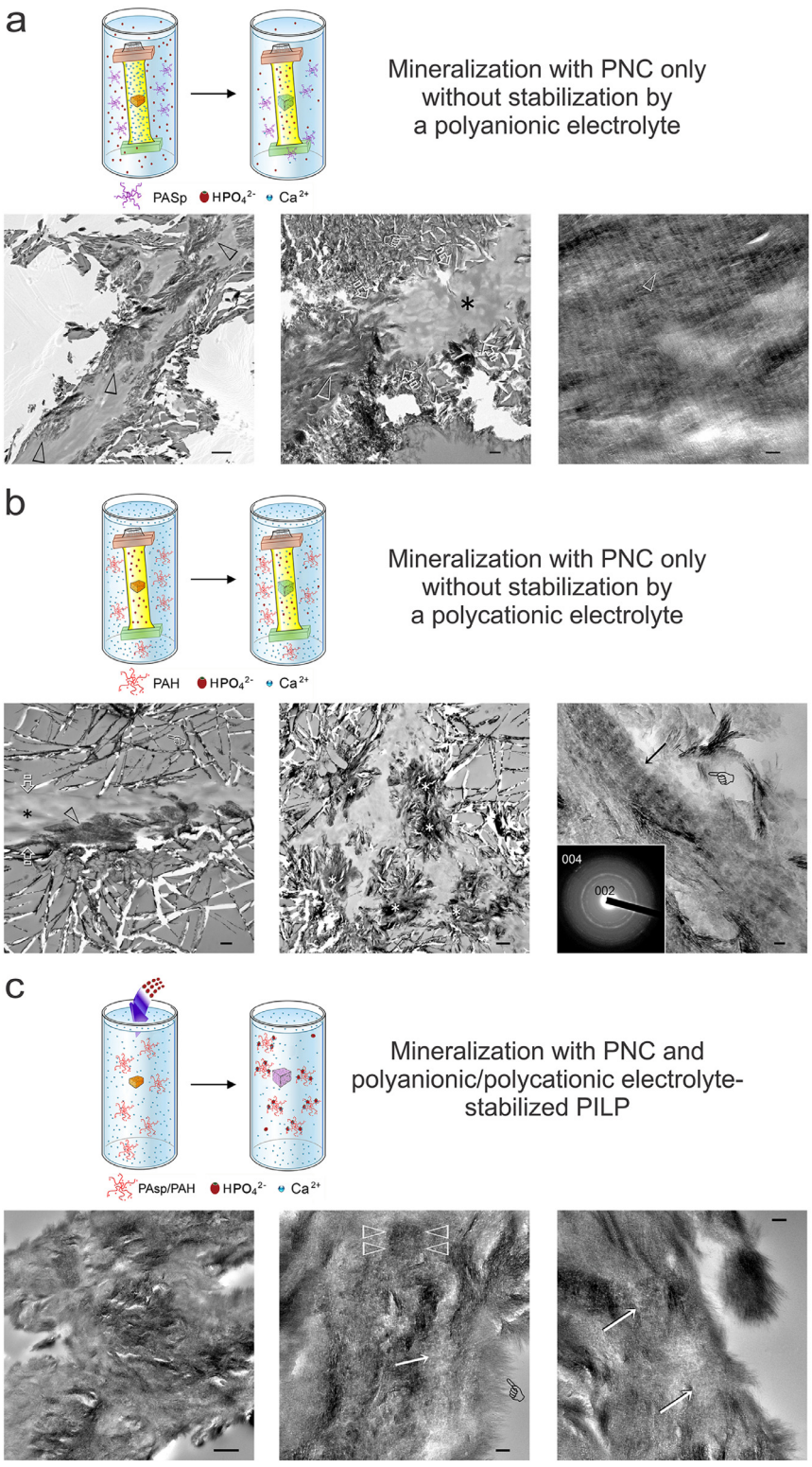

Fig. 3. TEM of non-osmicated, unstained sections prepared from epoxy resin-embedded mineralized collagen sponges. **a**. By PNCs in the absence of PAsp-stabilized PILPs. *Left.* A partially-mineralized collagen leaflet (bar: 1 μm) showing nodules of intrafibrillar mineralization (open arrowheads). *Middle.* A partially-mineralized leaflet (between open arrows; bar: 500 nm) showing an unmineralized region (asterisk) and a region with mineralized collagen fibrils (open arrowhead). Pointer: extrafibrillar mineral depositions on the surface of the leaflet. *Right.* Mineralized fibrils in the mineralized region (bar: 100 nm) with ordered deposition of intrafibrillar apatite crystallites (open arrowhead). **b**. By PNCs in the absence of PAH-stabilized PILPs. *Left.* A partially-mineralized collagen leaflet (between open arrows) within the collagen matrix (bar: 500 nm). Open arrowhead: collagen fibrils with intrafibrillar mineralization. Asterisk: unmineralized collagen fibrils. Pointer: "extrafibrillar mineral depositions on the leaflet surface. *Middle.* Cross-section of a partially-mineralized collagen leaflet (bar: 100 nm) showing nodules of intrafibrillar mineralization (asterisks). *Right.* A banded mineralized fibril showing individual mineral platelets (arrow) within the fibril (bar: 50 nm). Pointer: larger extrafibrillar mineral deposits. Inset: selected area electron diffraction of the mineralized fibril showing diffraction patterns characteristic of apatite. **c**. By a combination of PNC and nucleation inhibitor-stabilized PILP. *Left.* Heavily-mineralized collagen leaflet retrieved after 7 days of mineralization (bar: 500 nm). *Middle.* Intrafibrillar mineralization within longitudinally-sectioned (arrow) and cross-sectioned (between arrowheads) collagen fibrils (bar: 100 nm). *Right.* Less heavily-mineralized collagen fibrils along the periphery of a leaflet (bar: 50 nm) showing cross-banded mineralization patterns (arrows).

Please cite this article as: Y.-x. Ma, S.E. Hoff and X.-q. Huang et al., Involvement of prenucleation clusters in calcium phosphate mineralization of collagen, Acta Biomaterialia, https://doi.org/10.1016/j.actbio.2020.07.038

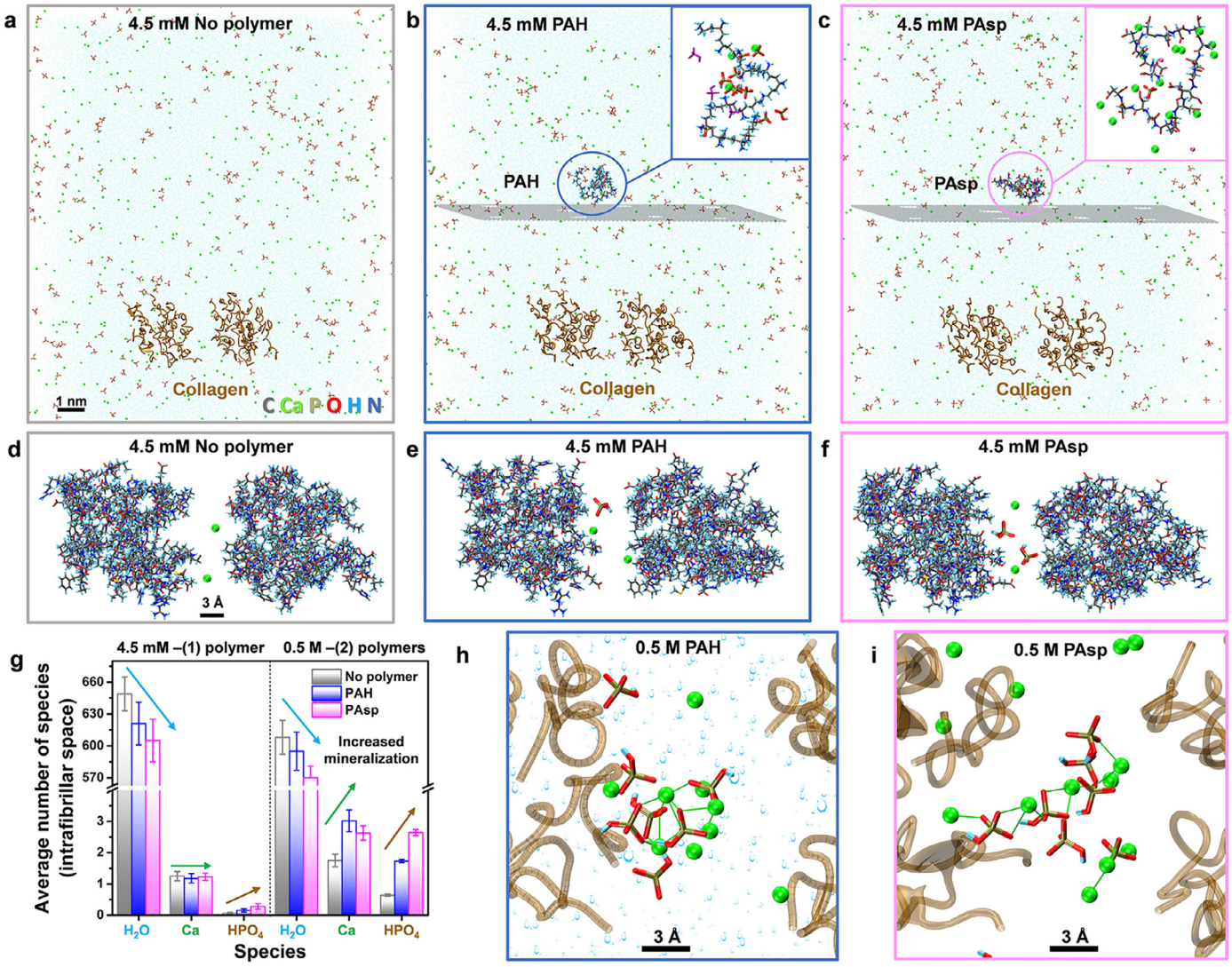

Fig. 4. Molecular dynamics simulations identified the role of polymeric nucleation inhibitors. The external polymers induce more ions to enter into the intrafibrillar collagen gap zone and form PNCs. **a-c**. Snapshots of equilibrium conformations for the polymer-free (gray boarder), single-PAH (blue border) and single PAsp (mauve border) collagen solution with a low concentration of Ca^{2+} of 4.5 mM and HPO_4^{2-} of 2.1 mM. A semipermeable membrane (500 Da MWCO) is included and collagen microfibrils are presented in ochre "cartoon" style. Additional Na^+ and Cl^- ions (including Cl^- excess for charge neutrality) are omitted for clarity. Twenty-monomer PAH and PAsp molecules are located at the left top corner. One backbone carbon atom of PAH and PAsp was fixed to prevent permeation through the membrane. Polymer and membrane are moved closer to collagen for ease of visualization. Water molecules in the system are shown as light blue dots. The insets in panel **b** and **c** represent enlarged views of the ions around PAH and PAsp in the encircled areas. PAH draws more hydrogen phosphate and PAsp more calcium ions into their immediate vicinity, respectively. d**–f**. Zoom-in of the side-view of the collagen intrafibrillar environment in **a-c** using the "licorice" drawing method. Ions inside the collagen fibril gap zone are highlighted with a larger size and remain largely isolated from each other. Water molecules are omitted for clarity. **g**. Comparison of the average amount of intrafibrillar water molecules and ions (Ca^{2+}, HPO_4^{2-}, Na^+ and Cl^-) for the control solution without polymer as well as the solutions containing PAH and PAsp. The distribution of Na^+ and Cl^- ions is not shown. **h, i**. Snapshots of CaP-PNC formed in the collagen gap zone in the presence of two PAH polymers (**h**) and two PAsp polymers (**i**) at high ion concentration of 0.5 M Ca^{2+} and 0.23 M HPO_4^{2-}. Na^+ and Cl^- ions are omitted for clarity. Distances of Ca^{2+} ions to the oxygen atoms of HPO_4^{2-} ions within 3 Å are highlighted by green bonds.

of Ca^{2+} ions in the intrafibrillar space, however, is already high because the majority of Ca^{2+} ions is bound to carboxylate side-groups inside the collagen fibril and remained about the same in the presence of the polymers. With increase in polymer concentration (addition of one more molecule) and increase in ion concentration (0.5 M Ca^{2+}, 0.23 M HPO_4^{2-}), the intrafibrillar ionic content increased and the number of water molecules was reduced, compared to that observed in the simulation with 4.5 mM Ca^{2+} ion concentration. The absolute number of intrafibrillar Ca^{2+}ions in the polymer-containing solutions was considerably higher than in the polymer-free solutions (Fig. 4g).

Taken together, inclusion of the nucleation inhibitors PAH and PAsp outside the semipermeable membrane leads to chelation of phosphate and calcium ions and reduce the volume of water in the inside the dialysis bag. Thereby, the mineralization conditions inside the dialysis bag change, increasing the concentration of CaP and accelerating the formation of PNCs inside the solution and in the intrafibrillar spaces of collagen. The use of PAsp was more effective than PAH to concentrate electrolytes, especially HPO_4^{2-} ions, in the collagen gap zone (Fig. 4g). The differences in polymer performance may be explained in terms of the closely-attracted ion shells, whereby the effectiveness in promoting intrafibrillar PNCs was higher for PAsp on a per-mole basis.

At only 4.5 mM Ca^{2+} concentration, formation of PNCs in solution and inside the fibril was difficult to observe using MDS. This was related to the limited accessible time scale compared to experiments. Accordingly, a higher supersaturated concentration of 0.5 M Ca^{2+} and twice the polymer concentration was tested to

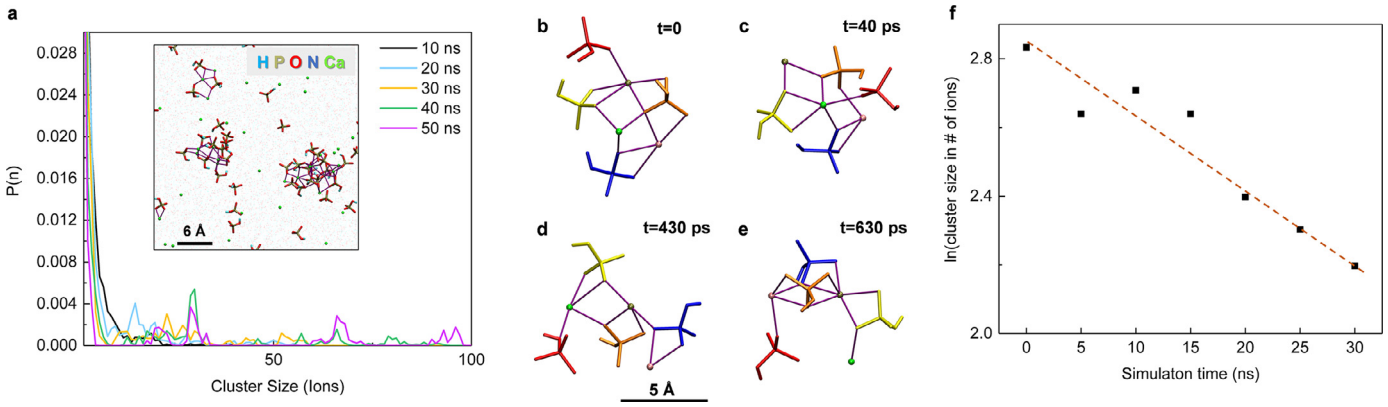

Fig. 5. Molecular dynamics simulations were performed to probe the existence of PNCs in calcium phosphate solutions and in the collagen intrafibrillar space. A solution of Ca^{2+} and $HPO4^{2-}$ in water was simulated at a supersaturated concentration of 0.5 M to accelerate the dynamics and monitor formation of PNCs. **a.** probability distribution of finding a calcium hydrogen phosphate cluster of a certain size as a function of time. Peaks shift to higher values with time, while peaks at small to intermediate cluster sizes exist throughout the simulation. This type of Flory distribution is predicted for PNCs as the lack of a phase boundary in the PNCs would entropically promote many different stable cluster sizes with no energetic penalty. Inset shows multiple PNC clusters at 30 ns. Magenta lines link Ca^{2+} and O of $HPO4^{2-}$ within a distance of 3 Å or less, corresponding to the Ca-O radius distribution function (RDF) to aid visualization. **b-e.** PNCs consisting of 4 units of $Ca^{2+}/HPO4^{2-}$ ion pairs were moved from the supersaturated 0.5 M Ca^{2+} solution into 18 mM Ca^{2+} solution to verify the stability and cluster dynamics. System displayed stability in solution on the nanosecond time scale but changed conformation on the 100 ps time scale. The small clusters quickly changed configurations within hundreds of picoseconds and individual ions within the small clusters in dilute solution occasionally dissociated at the start of simulations, but regularly returned to the cluster after a short period of time. A PNC composed of 3 Ca^{2+} ions and 4 $HPO4^{2-}$ ions in 18 mM solution is shown in **b-e.** Molecules are drawn with unique colors to better visualize conformational changes. The observed dynamics and stability of the clusters were similar at supersaturated concentration and at the less concentrated concentration equivalent to the experimental condition. **f.** Natural log of the cluster size of a 17 ion cluster as a function of time in 18 mM CaP solution. The PNC cluster stochastically breaks apart slowly with time. The slope of the plot gives a dissolution rate of −0.021 ions ns^{-1}. The CaP clusters observed in the simulations thus show all the characteristics expected for PNCs, such as Flory-like size distribution, absence of phase boundary, and dynamic stability.

shorten the time for prenucleation, which enabled direct observation of PNC during MDS. In the control solution without nucleation inhibitors, several hydrated PNCs of $Ca^{2+}$and HPO_4^{2-} ions were formed within the first 50 ns (Fig. 5a). The PNCs assume a size of several ions and grew up to 100 ions over time, while small to intermediate cluster sizes remained throughout the simulation. It is worth noting that there was not a defined amount of water per PNC. This Flory distribution of sizes, the lack of a phase boundary, and dynamic stability of many different cluster sizes with no energetic penalty, confirmed PNC formation in the simulation. This was also supported by the high reliability of IFF for phosphate minerals (Fig. 5b–e) [41,42]. The stability of a 17-ion PNC cluster was tested by placing it into 18 mM solution, representative of experimental concentrations, and allowing it to run for 30 ns (Fig. 5f). Similar to recent simulation results on $CaCO_3$ systems [46], the cluster was observed to stochastically break apart with time. However, the dissociation rate of the CaP PNC was found to be significantly slower than for previously reported $CaCO_3$ at the same concentration (−0.02 ions ns^{-1} vs −0.1 ions ns^{-1} respectively), and slow enough to provide time for some PNCs to reach intrafibrillar space in collagen where they can be stabilized. Prenucleation clusters were also observed in the presence of PAsp and PAH, wherein the local density of water was lower in the PNCs in the nucleation inhibitor-free solution (SI-6a, b) relative to PNCs in PAH and PAsp solutions (SI-6c-f). These findings support the attraction of a large portion of HPO_4^{2-} ions to PAH, and an even a larger portion of Ca^{2+} ions to PAsp, which increases the ionic strength outside the semipermeable membrane. Water is drained from the inside of the membrane via osmosis that is partially-extracted from the collagen intrafibrillar space and reduces the hydration level of collagen. The capacity to form stronger hydration shells increased in the order: no polymer < PAH < PAsp, and corresponds to the order of increased CaP concentration in the collagen intrafibrillar space. The simulation data offers a plausible mechanism for the cryo-EM results, that nucleation of HAp in collagen fibrils occurs with PNCs when PAsp and PAH are secluded from the mineralization milieu by a semipermeable membrane (Fig. 1). In case of a living organism with a bone fracture where osmolality is regulated, the externally-applied diaphragm (membrane) would maintain a concentration gradient and the polymers would continue to induce intrafibrillar mineralization. At the same time, more complex cellular electrolytes may also affect the activity.

Formation of PNCs in the intrafibrillar space, in our simplified collagen model systems, was also examined by MDS by increasing

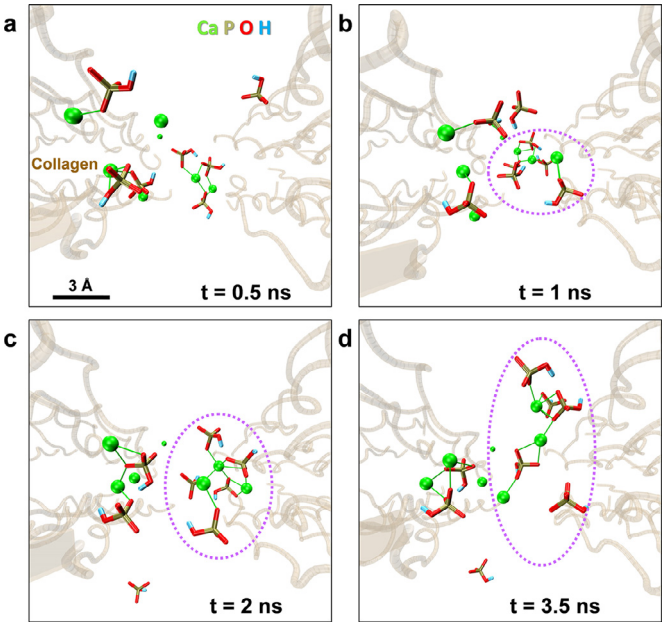

Fig. 6. Molecular dynamics simulations identified PNC formation within the intrafibrillar collagen gap zone. **a-d**. Perspective view snapshots of PNC conformation inside the intrafibrillar collagen gap zone for the PAsp system at different simulation times (t = 0.5, 1, 2, 3.5 ns). Distances of Ca^{2+} ions to oxygen atoms of HPO_4^{2-} ions within 3 Å are highlighted in green bonds. Collagen microfibrils are presented in ochre "cartoon" drawing method. Water, polymer molecules and ions are omitted for clarity. Dotted purple highlights indicate the conformation of PNC.

Please cite this article as: Y.-x. Ma, S.E. Hoff and X.-q. Huang et al., Involvement of prenucleation clusters in calcium phosphate mineralization of collagen, Acta Biomaterialia, https://doi.org/10.1016/j.actbio.2020.07.038

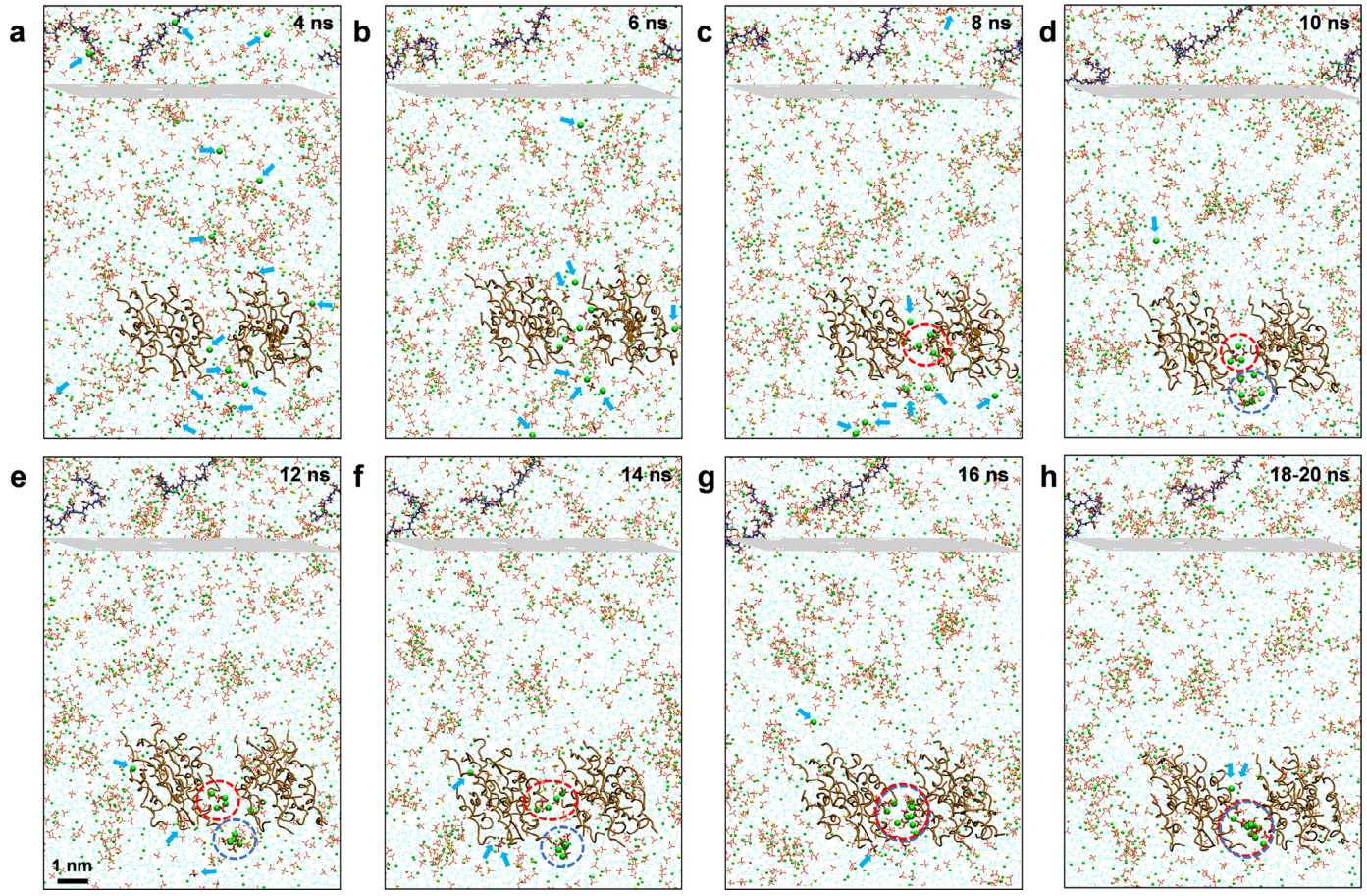

Fig. 7. Molecular dynamics simulations of the 0.5 M Ca^{2+}-PAsp system identified CaP-PNC conformations in solution and inside the collagen fibril. Ions that formed the intrafibrillar CaP-PNC are monitored and indicated by light-blue arrows. Collagen microfibrils are presented in the ochre "cartoon" drawing method. PAsp and HPO_4^{2-} ions are shown using the "licorice" drawing method. Calcium ions are shown in van der Waals style in green. Water molecules are shown in light-blue dots for clarification. Blue and red dotted lines distinguish the conformation of PNC inside the collagen and in solution, respectively.

the concentration of Ca^{2+} and HPO_4^{2-} ions to 0.5 M and 0.23 M, respectively (Fig. 3h, i). Initially, the ions were randomly dispersed in the gap zone and ion aggregation occurred over time in the collagen intrafibrillar gap zone. Ion aggregation began with the formation of smaller clusters (2 Ca^{2+} and 3 HPO_4^{2-}, 1 Ca^{2+} and 2 HPO_4^{2-}) and ion-pairs (1 Ca^{2+} and 1 HPO_4^{2-}) after 0.5 ns (Fig. 6a). Subsequently, more ions aggregated to form larger stable clusters (3 Ca^{2+} and 5 HPO_4^{2-}) after 1 ns (purple highlights in Fig. 6b). The PNCs were highly dynamic entities that changed their shape over time (Fig. 6b-d), including reorganization (SI-7) within the time scale of typical of molecular rearrangements in solution. Another example of reorganization was that PNCs released a HPO_4^{2-} ion and remained stable in solution (Fig. 5d) [28,38].

Intrafibrillar formation of PNCs was monitored during a simulation time of 20 ns in the supersaturated 0.5 M Ca^{2+} hydrogen phosphate-collagen-PAsp solution (Fig. 7). At the outset, all ions were evenly-distributed in the model system. Ions began to aggregate after 4 ns (Fig. 7a). As the MDS progressed, more ions entered the collagen gap zone (Fig. 7b). At 8 ns, an intrafibrillar PNC was formed (red dotted highlight in Fig. 7c). At 10 ns, more ions that gathered at the end of the collagen aggregated and formed another PNC, as indicated by blue dotted line in Fig. 7d. These two PNCs changed their conformation as simulation time increased (Fig. 7e-f). From 16 ns onwards, the two PNCs merged into one PNC and stayed inside the collagen gap zone for 4 ns (Fig. 7g–h). A movie depicting the formation of PNCs inside the collagen fibril gap zone can be found in SI-8.

In the absence of stabilization by nucleation inhibitors, PNCs in 0.5 M solution without collagen continued to aggregate into a single large ACP cluster after 200 ns of MDS simulation SI-9a, b). In the presence of PAsp, 1-2 nm large ACP clusters form around the polymer. However, the clusters do not aggregate after 200 ns of simulation, unlike those in the control system with no polymer. The result highlights the role of the polymer in preventing further aggregation and crystallization of ACP. (SI-9c, d) These are the first PILP structures found through MD and are remarkably similar to the miscroscale description of amorphous calcium carbonate PILPs found through recent cryoTEM studies (SI-10) [31]. While one would certainly expect the non-stabilized, densified CaP intermediates to crystallize with time, MDS of such a phenomenon would necessitate the use of long time scales (i.e. beyond the second range) that are currently not feasible using supercomputing, unless incorporating simulated annealing to speed-up the crystallization process. Simulated annealing is not suitable for the present systems, however, as it may result in denaturation and gelation of the collagen model [47]. Although MDS of crystallization from solution has been reported in the literature [48], a simple solute-solvent model system consisting of 500 solute and 3000 solvent particles was employed. In contrast, the present system includes collagen fibrillar structures in mineralization and is much larger and considerably more complex, drastically increasing computational cost.

High concentrations of calcium and phosphate ions beyond their physiologic concentrations had been used for collagen mineralization during *in vitro* fibrillogenesis without the use of nu-

cleation inhibitors to generate PILPs [5]. Using molecular dynamics simulation, Landis and coworkers predicted the formation of salt-bridge nests via electrostatic interaction of calcium phosphate ions with the charged amino acid side, chains of tropocollagen molecules [49]. Within the collagen fibril mineralization template [50], the salt-bridges act as nodules that initiate CaP precipitation within the gap zones of collagen fibrils without involvement of PILPs [50]. Although the results reported in those studies are stimulating, they are conducted either with extreme hyperosmolarity [5] or without direct experimental backup [50]. Because collagen fibrils behave as selectively-permeable membranes [51], polyanionic or polycationic polymers participate in intrafibrillar collagen mineralization by establishing a balance between osmosis and equilibration of electrical charges (i.e. Donnan equilibrium) in the vicinity of the collagen fibril to initiate infiltration of mineralization precursors [6]. This mineralization mechanism also suggests that unstabilized PNCs may be directly involved in collagen mineralization. We conclude that the combination of experimental and theoretical studies, using validated potentials [42], is important to understand the concept of unstabilized PNCs in non-classical nucleation.

The use of a semipermeable membrane for preventing a high molecular weight cationic or anionic nucleation inhibitor from forming PILPs in the vicinity of collagen fibrils should not be viewed upon as an alternative tissue engineering method for producing mineralized collagen. The environment within a semipermeable membrane does not offer the most favorable biomimetic conditions for inducing collagen intrafibrillar mineralization. It simply provides the means for examining whether intrafibrillar mineralization can be initiated by PNCs in already-assembled fibrillar collagen, in the absence of PILPs as stabilized amorphous intermediates. Being the smallest negatively-charged, hydrated particulate entities identifiable by cryo-EM in a CaP solution, the possibility of PNCs in collagen intrafibrillar mineralization has been speculated but never been clarified experimentally in circumstances where the osmolarity of CaP is within normal physiological range. Establishment of Donnan equilibrium using the semipermeable experiment design, albeit metastable compared with the conditions prevailing in the control, is conducive to the infiltration of PNC into fibrillar collagen. With redistribution of Ca^{2+} and HPO_4^{2-} ions and water across the selectively-permeable membrane to establish electrical neutrality and osmotic equilibrium, intrafibrillar mineralization of collagen is possible with PNCs alone. There is only a narrow window of opportunity for intrafibrillar mineralization to occur before extrafibrillar crystallization kicks in. Compared with conventional PILP-based intrafibrillar mineralization, mineralization of collagen fibrils using unstabilized PNCs is inefficient, as demonstrated by the mineralization of 3-D collagen matrices. In the absence of a nucleation inhibitor/processing directing agent, intrafibrillar mineralization by unstabilized PNCs is constrained by competition from extrafibrillar mineral deposition. Nevertheless, the narrow window of opportunity for PNCs to produce intrafibrillar mineralization provides a plausible explanation for the feasibility of nucleation inhibitor-free intrafibrillar apatite assembly during reconstitution of type I collagen [5]. The observations of prenucleation species alone challenge the classical nucleation theory and provide the basis for further research on multi-stage crystal nucleation processes.

4. Conclusion

The mechanism of intrafibrillar mineralization of collagen with PNCs alone is unraveled by cryo-EM and molecular dynamics simulation using a model system with a semipermeable membrane that helped establish Donnan equilibrium. The detailed dynamics of PNCs of calcium phosphates and atomic-level insights into the structure of PILPs are revealed by simulations in all-atom resolution in agreement with the experimental data. Compared with conventional PILP-based intrafibrillar mineralization, mineralization of collagen fibrils using unstabilized PNCs is possible, albeit inefficient. Inefficient mineralization is attributed to competition from extrafibrillar mineral deposition. Molecular dynamics simulations of the processes of PNC infiltration into a collagen fibril provide mechanistic understanding and suggest water extraction by the external PILPS as a likely reason for increased mineralization activity in the intrafibrillar space. Quantitative insights from simulations are promising to support further integrated mineralization studies across scales.

Declaration of Competing Interest

The authors declare that they have no known competing financial interests or personal relationships that could have appeared to influence the work reported in this paper.

Acknowledgments

The present work was supported by grants 81722015, 81870805, 81970959 and 81720108011 from National Nature Science Foundation of China and grant 2020TD-033 from the Shaanxi Key Scientific and Technological Innovation Team. We acknowledge support from the National Science Foundation (DMREF 1623947 and CBET 1530790, OAC 1931587, CMMI 1940335). This work also utilized the Summit supercomputer, a joint effort of the University of Colorado Boulder and Colorado State University, which is supported by the National Science Foundation (ACI-1532235 and ACI-1532236) and the Argonne Leadership Computing Facility, which is a DOE Office of Science User Facility supported under Contract DE-AC02–06CH11357.

Supplementary materials

Supplementary material associated with this article can be found, in the online version, at doi:10.1016/j.actbio.2020.07.038.

References

[1] M.J. Olszta, X. Cheng, S.S. Jee, R. Kumar, Y.Y. Kim, M.J. Kaufman, E.P. Douglas, L.B. Gower, Bone structure and formation: a new perspective, Mater. Sci. Eng. R. 58 (2007) 77–116.
[2] P.A. Price, D. Toroian, J.E. Lim, Mineralization by inhibitor exclusion the calcification of collagen with fetuin, J. Biol. Chem. 284 (2009) 17092–17101.
[3] F. Nudelman, K. Pieterse, A. George, P.H. Bomans, H. Friedrich, L.J. Brylka, P.A. Hilbers, G.de With, N.A. Sommerdijk, The role of collagen in bone apatite formation in the presence of hydroxyapatite nucleation inhibitors, Nat. Mater. 9 (2010) 1004–1009.
[4] F.H. Silver, W.J. Landis, Deposition of apatite in mineralizing vertebrate extracellular matrices: a model of possible nucleation sites on type I collagen, Connect. Tissue. Res. 52 (2011) 242–254.
[5] Y. Wang, T. Azaïs, M. Robin, A. Vallée, C. Catania, P. Legriel, G. Pehau-Arnaudet, F. Babonneau, M.M. Giraud-Guille, N. Nassif, The predominant role of collagen in the nucleation, growth, structure and orientation of bone apatite, Nat. Mater. 11 (2012) 724–733.
[6] L.N. Niu, S.E. Jee, K. Jiao, L. Tonggu, M. Li, L. Wang, Y.D. Yang, J.H. Bian, L. Breschi, S.S. Jang, J.H. Chen, D.H. Pashley, F.R. Tay, Collagen intrafibrillar mineralization as a result of the balance between osmotic equilibrium and electroneutrality, Nat. Mater. 16 (2017) 370–378.
[7] F. Nudelman, A.J. Lausch, N.A. Sommerdijk, E.D. Sone, In vitro models of collagen biomineralization, J. Struct. Biol. 183 (2013) 258–269.
[8] L.B. Gower, Chapter 6 - Biomimetic mineralization of collagen, in: C. Aparicio, M.P. Ginebra (Eds.), Biomineralization and Biomaterials: Fundamentals and Applications, 1st Edition, Woodhead Publishing, Elsevier Ltd., Cambridge, United Kingdom, 2016, pp. 187–232.
[9] K. Jiao, L.N. Niu, C.F. Ma, X.Q. Huang, D.D. Pei, T. Luo, Q. Huang, J.H. Chen, F.R. Tay, Complementarity and uncertainty in intrafibrillar mineralization of collagen, Adv. Funct. Mater. 26 (2016) 6858–6875.
[10] S. Karthika, T.K. Radhakrishnan, P. Kalaichelvi, A review of classical and nonclassical nucleation theories, Cryst. Growth Des. 16 (2016) 6663–6681.
[11] D. Zahn, Thermodynamics and kinetics of prenucleation clusters, classical and non-classical nucleation, ChemPhysChem 16 (2015) 2069–2075.

[12] L. Bergström, E.V. Sturm née Rosseeva, G. Salazar-Alvarez, H. Cölfen, Mesocrystals in biominerals and colloidal arrays, Acc. Chem. Res. 48 (2015) 1391–1402.
[13] A. Akiva, M. Kerschnitzki, I. Pinkas, W. Wagermaier, K. Yaniv, P. Fratzl, L. Addadi, S. Weiner, Mineral formation in the larval zebrafish tail bone occurs via an acidic disordered calcium phosphate phase, J. Am. Chem. Soc. 138 (2016) 14481–14487.
[14] P.R. ten Wolde, D. Frenkel, Enhancement of protein crystal nucleation by critical density fluctuations, Science 277 (1997) 1975–1978.
[15] N.D. Loh, S. Sen, M. Bosman, S.F. Tan, J. Zhong, C.A. Nijhuis, P. Král, P. Matsudaira, U. Mirsaidov, Multistep nucleation of nanocrystals in aqueous solution, Nat. Chem. 9 (2017) 77–82.
[16] J.J. De Yoreo, P.U. Gilbert, N.A. Sommerdijk, R.L. Penn, S. Whitelam, D. Joester, H. Zhang, J.D. Rimer, A. Navrotsky, J.F. Banfield, A.F. Wallace, F.M. Michel, F.C. Meldrum, H. Cölfen, P.M. Dove, Crystallization by particle attachment in synthetic, biogenic, and geologic environments, Science 349 (2015) aaa6760.
[17] A. Dey, P.H. Bomans, F.A. Müller, J. Will, P.M. Frederik, G. de With, N.A. Sommerdijk, The role of prenucleation clusters in surface-induced calcium phosphate crystallization, Nat. Mater. 9 (2010) 1010–1014.
[18] D. Zahn, Mechanisms of calcium and phosphate ion association in aqueous solution, Z. Anorg. Allg. Chem. 630 (2004) 1507–1511.
[19] W.J. Habraken, J. Tao, L.J. Brylka, H. Friedrich, L. Bertinetti, A.S. Schenk, A. Verch, V. Dmitrovic, P.H. Bomans, P.M. Frederik, J. Laven, P. van der Schoot, B. Aichmayer, G. de With, J.J. DeYoreo, N.A. Sommerdijk, Ion-association complexes unite classical and non-classical theories for the biomimetic nucleation of calcium phosphate, Nat. Commun. 4 (2013) 1507.
[20] Q. Zhang, Y. Jiang, B.D. Gou, J. Huang, Y.X. Gao, J.T. Zhao, L. Zheng, Y.D. Zhao, T.L. Zhang, K. Wang, In situ detection of calcium phosphate clusters in solution and wet amorphous phase by synchrotron X-Ray absorption near-edge spectroscopy at calcium K-edge, Cryst. Growth Des. 15 (2015) 2204–2210.
[21] G. Mancardi, U. Terranova, N.H. de Leeuw, Calcium phosphate prenucleation complexes in water by means of ab initio molecular dynamics simulations, Cryst. Growth Des. 16 (2016) 3353–3358.
[22] G. Mancardi, C.E.H. Tamargom, D.Di. Tommaso, N.H. de Leeuw, Detection of Posner's clusters during calcium phosphate nucleation: a molecular dynamics study, J. Mater. Chem. B. 5 (2017) 7274–7284.
[23] A. Carino, C. Ludwig, A. Cervellino, E. Müller, A. Testino, Formation and transformation of calcium phosphate phases under biologically relevant conditions: experiments and modelling, Acta Biomater. 1 (2018) 478–488.
[24] M.A. Bewernitz, D. Gebauer, J. Long, H. Cölfen, L.B. Gower, A metastable liquid precursor phase of calcium carbonate and its interactions with polyaspartate, Faraday Discuss. 159 (2012) 291–312.
[25] A.F. Wallace, L.O. Hedges, A. Fernandez-Martinez, P. Raiteri, J.D. Gale, G.A. Waychunas, S. Whitelam, J.F. Banfield, J.J. De Yoreo, Microscopic evidence for liquid-liquid separation in supersaturated $CaCO_3$ solutions, Science 341 (2013) 885–889.
[26] Z. Zou, I. Polishchuk, L. Bertinetti, B. Pokroy, Y. Politi, P. Fratzl, W.J.E.M. Habraken, Additives influence the phase behavior of calcium carbonate solution by a cooperative ion-association process, J. Mater. Chem. B. 6 (2018) 449–457.
[27] D. Gebauer, M. Kellermeier, J.D. Gale, L. Bergström, H. Cölfen, Pre-nucleation clusters as solute precursors in crystallization, Chem. Soc. Rev. 43 (2014) 2348–2371.
[28] D. Gebauer, How can additives control the early stages of mineralization? Minerals 8 (2018) 179.
[29] A. Veis, J.R. Dorvee, Biomineralization mechanisms: a new paradigm for crystal nucleation in organic matrices, Calcif. Tissue Int. 93 (2013) 307–315.
[30] A.S. Schenk, H. Zope, Y.Y. Kim, A. Kros, N.A.J.M. Sommerdijkc, F.C. Meldrum, Polymer-induced liquid precursor (PILP) phases of calcium carbonate formed in the presence of synthetic acidic polypeptides - Relevance to biomineralization, Faraday Discuss. 159 (2012) 327–344.
[31] Y. Xu, K.C.H. Tijssen, P.H.H. Bomans, A. Akiva, H. Friedrich, A.P.M. Kentgens, N.A.J.M. Sommerdijk, Microscopic structure of the polymer-induced liquid precursor for calcium carbonate, Nat. Commun. 9 (2018) 2582.
[32] S.J. Homeijer, R.A. Barrett, L.B. Gower, Polymer-induced liquid-precursor (PILP) process in the non-calcium based systems of barium and strontium carbonate, Cryst. Growth Des. 10 (2010) 1040–1052.
[33] T.T. Thula, F. Svedlund, D.E. Rodriguez, J. Podschun, L. Pendi, L.B. Gower, Mimicking the nanostructure of bone: comparison of polymeric process-directing agents, Polymers (Basel) 3 (2011) 10–35.
[34] Y. Li, C. Aparicio, Discerning the subfibrillar structure of mineralized collagen fibrils: a model for the ultrastructure of bone, PLoS ONE 8 (2013) e76782.
[35] A. Rao, H. Cölfen, Mineralization and non-ideality: on nature's foundry, Biophys. Rev. 8 (2016) 309–329.
[36] D. Gebauer, M. Kellermeier, J.D. Gale, L. Bergström, H. Cölfen, Pre-nucleation clusters as solute precursors in crystallization, Chem. Soc. Rev. 43 (2014) 2348–2371.
[37] D. Erdemir, A.Y. Lee, A.S. Myerson, Nucleation of crystals from solution: classical and two-step models, Acc. Chem. Res. 42 (2009) 621–629.
[38] R. Demichelis, P. Raiteri, J.D. Gale, D. Quigley, D. Gebauer, Stable prenucleation mineral clusters are liquid-like ionic polymers, Nat. Commun. 2 (2011) 590.
[39] J. Chen, E. Zhu, J. Liu, S. Zhang, Z. Lin, X. Duan, H. Heinz, Y. Huang, J.J. De Yoreo, Building two-dimensional materials one row at a time: avoiding the nucleation barrier, Science 362 (2018) 1135–1139.
[40] J. Zhou, Y. Yang, Y. Yang, D.S. Kim, A. Yuan, X. Tian, C. Ophus, F. Sun, A.K. Schmid, M. Nathanson, H. Heinz, Q. An, H. Zeng, P. Ercius, J. Miao, Nature accepted for publication, https://arxiv.org/abs/1807.10709.
[41] T.Z. Lin, H. Heinz, Accurate force field parameters and pH resolved surface models for hydroxyapatite to understand structure, mechanics, hydration, and biological interfaces, J. Phys. Chem. C 120 (2016) 4975–4992.
[42] H. Heinz, T.J. Lin, R.K. Mishra, F.S. Emami, Thermodynamically consistent force fields for the assembly of inorganic, organic, and biological nanostructures: the Interface Force Field, Langmuir 29 (2013) 1754–1765.
[43] H. Heinz, H. Ramezani-Dakhel, Simulations of inorganic–bioorganic interfaces to discover new materials: insights, comparisons to experiment, challenges, and opportunities, Chem. Soc. Rev. 45 (2016) 412–448.
[44] S.S. Jee, T.T. Thula, L.B. Gower, Development of bone-like composites via the polymer-induced liquid-precursor (PILP) process. Part 1: influence of polymer molecular weight, Acta Biomater. 6 (2010) 3676–3686.
[45] J.P.D. Goldring, Concentrating Proteins by Salt, Polyethylene Glycol, Solvent, SDS Precipitation, Three-Phase Partitioning, Dialysis, Centrifugation, Ultrafiltration, Lyophilization, Affinity Chromatography, Immunoprecipitation or Increased Temperature for Protein Isolation, Drug Interaction, and Proteomic and Peptidomic Evaluation, in: B. Kurien, R. Scofield (Eds.), Electrophoretic Separation of Proteins. Methods in Molecular Biology, Humana Press, New York, 2009, pp. 41–59.
[46] P.J.M. Smeets, A.R. Finney, W.J.E.M. Habraken, F. Nudelman, H. Friedrich, J. Laven, J.J. De Yoreo, P.M. Rodger, N.A.J.M. Sommerdijk, A classical view on nonclassical nucleation, P. Natl. Acad. Sci. 114 (2017) 882–890.
[47] L. Bozec, M. Odlyha, Thermal denaturation studies of collagen by microthermal analysis and atomic force microscopy, Biophys. J. 101 (2011) 228–236.
[48] J. Anwar, P.K. Boateng, Computer simulation of crystallization from solution, J, Am. Chem. Soc. 120 (1998) 9600-0604.
[49] Z. Xu, Y. Yang, W. Zhao, Z. Wang, W.J. Landis, Q. Cui, N. Sahai, Molecular mechanisms for intrafibrillar collagen mineralization in skeletal tissues, Biomaterials 39 (2015) 59–66.
[50] W.J. Landis, F.H. Silver, J.W. Freeman, Collagen as a scaffold for biomimetic mineralization of vertebrate tissues, J. Mater. Chem. 16 (2006) 1495–1503.
[51] A. Maroudas, Balance between swelling pressure and collagen tension in normal and degenerate cartilage, Nature 260 (1976) 808–809.

Please cite this article as: Y.-x. Ma, S.E. Hoff and X.-q. Huang et al., Involvement of prenucleation clusters in calcium phosphate mineralization of collagen, Acta Biomaterialia, https://doi.org/10.1016/j.actbio.2020.07.038